J. Fluid Mech. (1999), *vol.* 393, *pp.* 333–356. Printed in the United Kingdom

Hysteretic response of supported drops during forced oscillations

By EDWARD D. WILKES AND OSMAN A. BASARAN†

School of Chemical Engineering, Purdue University, West Lafayette, IN 47907-1283, USA

(Received 23 May 1997 and in revised form 6 April 1999)

Viscous liquid drops undergoing forced oscillations have been shown to exhibit hysteretic deformation under certain conditions both in experiments and by solution of simplified model equations that can only provide a qualitative description of their true response. The first hysteretic deformation results for oscillating pendant drops obtained by solving the full transient, nonlinear Navier–Stokes system are presented herein using a sweep procedure in which either the forcing amplitude A or frequency Ω is first increased and then decreased over a given range. The results show the emergence of turning-point bifurcations in the parameter space of drop deformation versus the swept parameter. For example, when a sweep is carried out by varying Ω while holding A fixed, the first turning point occurs at $\Omega \equiv \Omega_u$ as Ω is being increased and the second one occurs at $\Omega \equiv \Omega_l < \Omega_u$ as Ω is being decreased. The two turning points shift further from each other and toward lower values of the swept parameter as Reynolds number Re is increased. These turning points mark the ends of a hysteresis range within which the drop may attain either of two stable steady oscillatory states – limit cycles – as identified by two distinct solution branches. In the hysteresis range, one solution branch, referred to as the upper solution branch, is characterized by drops having larger maximum deformations compared to those on the other branch, referred to as the lower solution branch. Over the range $\Omega_l \leqslant \Omega \leqslant \Omega_u$, the sweep procedure enables detection of the upper solution branch which cannot be found if initially static drops are set into oscillation as in previous studies of forced oscillations of supported and captive drops, or liquid bridges. The locations of the turning points and the associated jumps in drop response amplitudes observed at them are studied over the parameter ranges $0.05 \leqslant A \leqslant 0.125$, $20 \leqslant Re \leqslant 40$, and gravitational Bond number $0 \leqslant G \leqslant 1$. Critical forcing amplitudes for onset of hysteresis are also determined for these Re values. The new findings have important ramifications in several practical applications. First, that $\Omega_u - \Omega_l$ increases as Re increases overcomes the limitation which is inherent to the current practice of inferring the surface tension and/or viscosity of a bridge/drop liquid from measurement of its resonance frequencies (Chen & Tsamopoulos 1993; Mollot *et al.* 1993). Moreover, that the value of A for onset of hysteresis can be as low as 5% of the drop radius, or lower, has important implications for other free-surface flows such as coating flows.

1. Introduction

There is growing interest in developing a fundamental understanding of forced oscillations of liquid bridges or captive drops (Borkar & Tsamopoulos 1991; Mollot *et*

† Author to whom correspondence should be addressed: e-mail: obasaran@ecn.purdue.edu.

al. 1993; Chen & Tsamopoulos 1993, hereafter referred to as C&T), pendant bubbles (Chang & Franses 1994*a*, *b*), supported – pendant and sessile – drops (DePaoli, Scott & Basaran 1992; Wilkes & Basaran 1997, hereafter referred to as W&B), and acoustically levitated drops (Daidžić 1995; Trinh, Holt & Thiessen 1996). The motivation for many of these studies comes from practical applications in diverse fields, examples of which include agglomeration of powders (Chen, Tsamopoulos & Good 1992; Tsamopoulos, Chen & Borkar 1992; C&T), measurement of the viscosity and surface tension of high-temperature materials (C&T; Basaran & DePaoli 1994), measurement of dynamic surface tension (Chang & Franses 1994*a*, *b*), mass transfer enhancement in electric field-assisted solvent extraction (Scott & Wham 1988; Ptasinski & Kerkhof 1992), electrospray methods for synthesis of ceramic precursor powders (Harris, Scott & Byers 1992), and two-phase heat transfer cells for micro-gravity based on vibration-induced atomization of supported drops (Smith *et al.* 1998).

When supported drops or their closely related analogues that are referred to in the previous paragraph are forced to undergo finite-amplitude oscillations at forcing frequency $\tilde{\Omega}$ and fixed forcing amplitude $\tilde{A}$, the largest interface deformation that the drop attains while undergoing steady-state oscillations during any oscillation period is maximized at a series of the value of the forcing frequency called resonance frequencies $\tilde{\omega}_{rn}$, where $n = 1, 2, \ldots$. W&B studied the forced oscillations of pendant and sessile drops that are induced by vibrating the substrate on which the drops are supported. W&B showed that the resonance frequencies depend strongly on drop size and properties and forcing amplitude. The deformation profiles, namely the curves of maximum drop deformation versus $\tilde{\Omega}$, that they obtained demonstrated the softening nonlinearity of the system, which was characterized by asymmetric skewing of the resonance peaks toward lower values of the frequency as the Reynolds number Re (while holding dimensionless forcing amplitude A fixed) or A (while holding Re fixed) increased. As first shown by C&T and Mollot *et al.* (1993) for liquid bridges, the computed variation of the resonance frequency with Re, which depends on viscosity, surface tension, density, and drop size, can be combined with its experimental measurement to infer the viscosity or the surface tension of the drop liquid. Unfortunately, the sensitivity of the resonance frequency to changes in Re becomes small and approaches zero as Re continues to increase, thereby rendering the technique useless for Reynolds numbers exceeding about 30.

For sufficiently large Re and/or A, W&B sometimes observed a finite jump in the value of maximum drop deformation when the forcing frequency was increased by a small amount: this indicates that there is the possibility of more than one stable solution to the nonlinear system of equations governing fluid motion inside the drop and drop shape at those parameter values, or that hysteresis may occur. The major goal of this paper is to investigate theoretically the conditions for the occurrence of hysteresis during forced oscillations of supported drops, which has not heretofore been attempted.

Hysteresis is the phenomenon whereby a system can have more than one stable solution, or response or output, for the same set of input parameters depending on the previous state of the system. Figure 1 illustrates a typical hysteretic response for a system with a soft nonlinearity, where x is the control parameter or the input and y represents the response parameter or the output. Points B and C show locations in parameter space at which turning-point bifurcations occur when the control parameter equals x_l and x_u, respectively. The broken curve joining B and C represents an unstable, and unobservable, solution branch. The upper and lower stable branches of solutions are depicted by the two solid curves. Points B and C thus

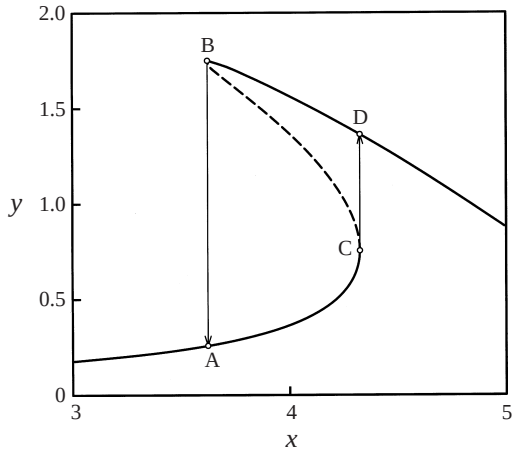

FIGURE 1. Typical hysteretic response that would be exhibited by the forced Duffing oscillator having a soft nonlinearity.

identify a hysteresis range of the control parameter $x_l \leqslant x \leqslant x_u$ within which more than one solution exists for the response parameter y. Outside this range only one solution exists.

Examples of systems for which hysteresis has been observed include the buckled beam (Pezeshki, Elgar & Krishna 1991), the damped unbalanced rotating shaft (Shaw & Shaw 1991), forced convective boiling (Salehpour & Yao 1983), and the semilinear phase-conjugate mirror (Królikowski & Cronin-Golomb 1991). Hysteresis is often an undesirable effect, as in the buckled beam example where the beam can undergo rapid oscillation between two stable states. Hysteresis is often also a cause of energy or efficiency loss, as in rolling friction (e.g. Koizumi *et al.* 1983). Yet another goal of this paper is to show that the phenomenon of hysteresis can be used to advantage in inferring the physical properties of the drop (bridge) liquid in forced oscillations of supported drops (liquid bridges) by overcoming the aforementioned limitation of the method that arises at even moderate values of *Re*.

While the computational work of W&B on supported drops and that of C&T on liquid bridges clearly have pointed to the possibility of hysteresis, these authors always started integrating their equations in time from an initially static rest state. Unfortunately, such an approach precludes insight into the effects of initial conditions. For a system which can exhibit hysteretic response, detection of a second limit cycle requires that the initial conditions or the previous state of the drop be varied in a systematic fashion. A convenient way of systematically varying initial conditions theoretically or experimentally is to carry out a discrete sweep procedure in which the control parameter, here the forcing frequency Ω or amplitude A, is varied from a low value to a high value and then back to the original low value. For example, when a sweep is carried out in forcing frequency, the governing equations are solved numerically at a given value of Ω until a limit cycle is detected. The steady oscillatory solution that is thereby obtained is then used as the initial condition for the solution when the sweep parameter is changed to $\Omega \pm \Delta\Omega$, where $\Delta\Omega$ is a specified increment.

Therefore, when the control parameter x is increased or decreased over a range during a sweep in which the system exhibits hysteresis as in figure 1, the observed value of the response parameter y follows one of the two stable solution branches

indicated by the solid curves until the turning point at the end of that branch is reached. When x is further varied in that direction beyond the turning point by an amount Δx, y jumps to the other branch regardless of how small Δx is. Hence, the jump in the response provides a convenient way for detecting the location of the turning points. This behaviour, which is also known as the jump phenomenon, is exhibited by simple nonlinear models such as the damped forced Duffing oscillator (Hagedorn 1981; Jordan & Smith 1987). By contrast, the response that would be uncovered by the previous method of W&B would consist solely of the complete lower solution branch up to point C and the portion of the upper branch to the right of point D.

DePaoli *et al.* (1995; see also DePaoli 1994) employed a sweep procedure and experimentally detected hysteretic response in the case of drops of mixtures of glycerin and water that are pendant from the tip of a capillary tube and forced to undergo oscillations by subjecting them to mechanical or electrical forcing. Although these authors characterized the transient deformation of the drops through a spectrophotometric technique, they also used a high-speed camera to obtain photographic evidence that confirmed that two stable oscillatory states are possible at the same value of the forcing frequency over a hysteresis range. The drop responses that they observed were qualitatively similar to that of the soft-nonlinear Duffing oscillator depicted in figure 1. These authors further demonstrated that hysteretic drop response can also be observed by performing a sweep in the forcing amplitude while holding fixed the forcing frequency, thereby examining the parameter space from an additional perspective. DePaoli (1994) curve-fitted his experimentally determined results exhibiting hysteresis to simple, low-order nonlinear models. He found that if the curve-fits are carried out by using experimental measurements from one region of the parameter space, the simple nonlinear models could not predict quantitatively the response of real drops in another region of the parameter space. The latter finding (*a*) should not be too surprising given that the multi-dimensional Navier–Stokes system is a partial differential equation that is much more complex than an equation that governs the dynamic response of a simple nonlinear oscillator and (*b*) further points to the need for solving numerically the full Navier–Stokes system for elucidating the hysteretic response of supported drops (liquid bridges).

Several other studies of drops and bubbles, albeit in the absence of solid supporting boundaries, have uncovered hysteretic response during forced oscillations. Parlitz *et al.* (1990) solved a one-dimensional equation to study the radial oscillations of a gas bubble suspended in water and subjected to forcing induced by an external, time-periodic sound field. Their results showed that such a bubble can can be driven into a hysteretic, or even chaotic, deformation response when the amplitude of the forcing is sufficiently large. Daidžić (1995) experimentally observed hysteretic deformation of a free drop of n-hexadecane that is acoustically levitated in air and forced to oscillate due to periodic variation of the acoustic pressure. This author also discovered that when the drop was oscillated about an equilibrium shape which is an oblate spheroid, it exhibited a hard nonlinearity such that the observed resonance frequencies increased with increasing excitation amplitude. Later, Trinh *et al.* (1996) observed hysteretic deformation with soft nonlinearity as shown in figure 1 in the case of small droplets of water/glycerin solutions that are acoustically levitated in air and forced to undergo oscillations due to imposition of time-periodic electric or acoustic fields. Another interesting nonlinear phenomenon that these authors observed is that the droplets may exhibit asymmetric shape instabilities in the vicinity of the lower turning point during a downward sweep. Therefore, although previous studies of

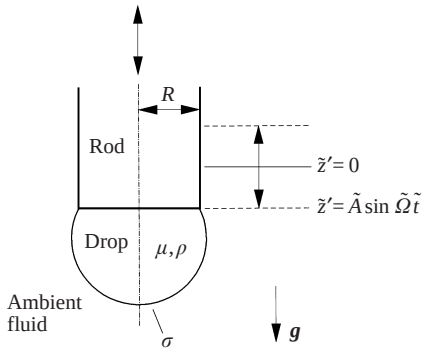

FIGURE 2. A liquid drop supported on a solid rod and undergoing forced oscillations in a vacuum or a gas of negligible density and viscosity.

nonlinear oscillations of drops and bubbles have uncovered hysteretic drop or bubble response, they have either been experimental in nature or entailed computational analysis of simple one-dimensional models.

Section 2 presents the problem statement and governing equations, boundary conditions, and initial conditions. The finite-element algorithm used and the discrete sweep procedure employed are explained in detail in § 3. Section 4 presents the first computational results for a pendant drop hanging from a rod that exhibits hysteretic response during forced oscillations. Section 4 ends by extending the present results to situations in which the drops are supported on a tube instead of a rod. Concluding remarks and the relevance of the new results to certain other practically important free-surface flows are given in § 5.

2. Problem statement

The system considered here is an axisymmetric drop of an incompressible Newtonian liquid of constant viscosity μ and density ρ that is pendant from a circular cylindrical rod of radius R. As shown in figure 2, the rod axis lies along the $\tilde{z}'$-direction and coincides with the axis of symmetry of the drop and the direction of gravity. The drop is forced into oscillations by oscillating the rod in the $\tilde{z}'$-direction sinusoidally in time with forcing frequency $\tilde{\Omega}$ and amplitude $\tilde{A}$ such that the the position $\tilde{z}'$ of the rod–drop interface in a fixed frame of reference is given by $\tilde{z}' = \tilde{A}\sin\tilde{\Omega}\tilde{t}$, where $\tilde{t}$ is time. Aside from exerting a constant pressure, the ambient gas surrounding the drop is taken to have a negligible influence on the dynamics. The drop/ambient fluid interface has constant surface tension σ, and is of course free to deform as the drop oscillates. However, the three-phase contact line is held fixed at, or is pinned to, the edge of the circular face of the rod. In what follows, whenever the same symbol is used to denote a dimensional quantity and its dimensionless counterpart, the dimensional quantity has a tilde above it and its dimensionless counterpart has not.

2.1. *Governing equations and boundary conditions*

The time-dependent motion of liquid within the drop volume V is governed by the Navier–Stokes system,

$$\nabla \cdot \boldsymbol{v} = 0 \quad \text{in} \quad V, \tag{1}$$

$$Re\left(\frac{\partial \boldsymbol{v}}{\partial t} + \boldsymbol{v}\cdot\nabla\boldsymbol{v} - A\Omega^2\sin(\Omega t)\,\boldsymbol{e}_z\right) = \nabla\cdot\boldsymbol{T} + Re\,G\,\boldsymbol{e}_z \quad \text{in} \quad V, \tag{2}$$

that is written in a non-inertial frame of reference in which the rod is stationary, i.e. $z = z' - A\sin\Omega t$. The dimensionless symbols used in the equations of conservation of mass (1) and momentum (2) are the gradient operator $\nabla \equiv R\tilde{\nabla}$, velocity $\boldsymbol{v} \equiv \sqrt{\rho R/\sigma}\,\tilde{\boldsymbol{v}}$, forcing amplitude $A \equiv \tilde{A}/R$, forcing frequency $\Omega \equiv \sqrt{\rho R^3/\sigma}\tilde{\Omega}$, time $t \equiv \sqrt{\sigma/\rho R^3}\,\tilde{t}$, and stress tensor $\boldsymbol{T} \equiv \sqrt{\rho R^3/\mu^2\sigma}\,\tilde{\boldsymbol{T}}$. For a Newtonian fluid, the total dimensionless stress is given by $\boldsymbol{T} = -p\boldsymbol{I} + [\nabla\boldsymbol{v} + (\nabla\boldsymbol{v})^T]$, where $p \equiv \sqrt{\rho R^3/\mu^2\sigma}\,\tilde{p}$ is the dimensionless pressure and $\boldsymbol{I}$ is the identity tensor. The dimensionless numbers that appear in (1) and (2) are the Reynolds number $Re \equiv (1/\nu)\sqrt{\sigma R/\rho}$ (see Basaran 1992), which represents the importance of inertial force relative to viscous force, and the gravitational Bond number $G \equiv \rho g R^2/\sigma$, which represents the importance of gravitational force relative to surface tension force. Here, g is the magnitude of gravitational acceleration, $\nu \equiv \mu/\rho$ is the kinematic viscosity, and unit vector $\boldsymbol{e}_z$ is in the axial direction. As in the previous work of W&B, it is found convenient here to cast the governing equations onto a spherical polar coordinate system (r, θ, ϕ) with its origin at the centre of the rod face, where ϕ is measured around the axis of symmetry.

Along the drop/ambient fluid interface $S(t)$, whose shape is expressed mathematically by $r - f(\theta, t) = 0$, the traction boundary condition demands that

$$\boldsymbol{n}_S \cdot \boldsymbol{T} = Re\,(2H)\,\boldsymbol{n}_S \quad \text{on} \quad S(t), \tag{3}$$

where $2H(\boldsymbol{x}_S, t)$ is twice the local mean curvature of $S(t)$, $\boldsymbol{x}_S \in S(t)$ is the position vector of points on the interface, and the outward unit normal to the surface is given by $\boldsymbol{n}_S = (f\boldsymbol{e}_r - f_\theta \boldsymbol{e}_\theta)/\sqrt{f^2 + f_\theta^2}$, where $f_\theta \equiv \partial f/\partial\theta$.

The drop shape, which is unknown *a priori*, is a material surface provided there is no mass transfer across it. Hence the kinematic condition demands that

$$\boldsymbol{n}_S \cdot (\boldsymbol{v} - \boldsymbol{v}_S) = 0 \quad \text{on} \quad S(t), \tag{4}$$

where $\boldsymbol{v}$ and $\boldsymbol{v}_S$ are the velocities of points located in V (just inside the surface) and on $S(t)$, respectively. Following Kistler & Scriven (1983) and W&B, equation (4) is treated as an additional governing equation and used to solve for the position of the free surface.

Because the oscillations are axisymmetric, the problem domain is simply the two-dimensional region $\{V : 0 \leqslant \theta \leqslant \pi/2; \quad 0 \leqslant r \leqslant f(\theta, t)\}$. Axial symmetry is imposed by requiring the vanishing of the partial derivative of the shape function with respect to the meridional angle at the drop tip

$$f_\theta = 0 \quad \text{at} \quad \theta = 0 \tag{5}$$

and the vanishing of both the θ-velocity and the shear stress along the drop centreline S',

$$\boldsymbol{n}' \cdot \boldsymbol{v} = 0 \quad \text{on} \quad S' \tag{6}$$

$$\boldsymbol{n}'\,\boldsymbol{t}' : \boldsymbol{T} = 0 \quad \text{on} \quad S' \tag{7}$$

where $\boldsymbol{n}'$ and $\boldsymbol{t}'$ are the unit vectors normal and parallel to the axis of symmetry S', respectively.

Because the contact line is pinned,

$$f = 1 \quad \text{at} \quad \theta = \pi/2\,. \tag{8}$$

Finally, the drop liquid must obey conditions of no-slip and no-penetration along the drop–rod interface,

$$\boldsymbol{v} = \boldsymbol{0} \quad \text{at} \quad \theta = \pi/2\,. \tag{9}$$

2.2. *Initial conditions*

Each sweep carried out in this paper is started from an initial static state such that the shape of the drop at $t = 0$ is a hemisphere of the same radius as the rod

$$f(\theta, t = 0) = 1\,, \tag{10}$$

and the liquid inside the drop is quiescent

$$\boldsymbol{v}(\boldsymbol{x}, 0) = \boldsymbol{0}, \quad p(\boldsymbol{x}, 0) = \text{constant} \quad \text{in} \quad V\,, \tag{11}$$

where $\boldsymbol{x} \in V$. Whereas W&B use (10) and (11) as initial conditions in obtaining a steady oscillatory solution at any value of the set of parameters $\{Re, G, A, \Omega\}$, these conditions are used here as initial conditions only when starting a frequency sweep at a value of $\Omega = \Omega_{\text{low}}$ while holding fixed the set of parameters $\{Re, G, A\}$ or when starting an amplitude sweep from a value of $A = A_{\text{low}}$ while holding fixed the set of parameters $\{Re, G, \Omega\}$. During a frequency sweep, for example, once a limit cycle is reached at $\Omega = \Omega_{\text{low}}$, the control parameter Ω is increased to $\Omega = \Omega_{\text{low}} + \Delta\Omega$ and the initial conditions on the drop shape and velocity and pressure fields within the drop at the new value of the control parameter are those of the limit-cycle solution attained at the previous value of the control parameter. This procedure is continued by increasing Ω at each step until a specified value of the control parameter Ω_{high} is reached. Thereafter, the systematic procedure of moving the system from one steady oscillatory state to a new steady oscillatory state is continued but now by decreasing the control parameter by an amount $\Delta\Omega$ at each step. The same procedure is employed during an amplitude sweep where the control parameter is first varied from A_{low} to A_{high} in increments of ΔA and then back to the starting point.

3. Finite-element analysis

The algorithm based on the Galerkin/finite-element method (G/FEM) and the FORTRAN program developed by W&B for analysis of pendant drop oscillations without hysteresis were modified to incorporate the sweep procedure described in the previous section and will be further elaborated below. The drop interior was divided into a mesh of N_θ by N_r biquadratic elements in the meridional (θ) and radial (r) directions (cf. W&B). In this section, only those aspects of the algorithm that differ from those of W&B are described. For details of code development and computer implementation, the reader is referred to W&B. The resulting modified code was run on IBM RS6000-320H and 590 workstations and a Silicon Graphics (SGI) Indigo II Extreme R4400 workstation at the Oak Ridge National Laboratory and an SGI Indigo II Extreme R8000 workstation at Purdue University.

3.1. *Volume conservation and accuracy tests*

In previous studies of free and forced oscillations of liquid drops and bridges in which numerical methods that are similar to the ones used in this work were employed, the discretized equations were integrated in time for at most a few hundred time steps (Basaran 1992; C&T; Basaran & DePaoli 1994). However, detection of a single limit cycle solution can require on the order of 1000 time steps and a typical sweep often lasts on the order of 10 000 or more time steps in this work. The criterion that is used here to determine that a steady oscillatory state has been reached at each value of Ω or A is that the maximum values of the drop aspect ratio $(a/b)_m$, where the aspect ratio $(a/b) \equiv f(0, t)/f(\pi/2, t)$, during the last three oscillation periods agree

to within a tolerance of 5×10^{-4}. Although the drop typically undergoes tens of periods of oscillation during 1000 time steps, the drop volume deviates by less than 0.1% from its original value during this time period. However, since the computations for a typical sweep require an order of magnitude more time steps, there exists the possibility that small errors in drop volume which occur at each time step might accumulate over a simulation and prevent the detection of a limit cycle in certain regions of the parameter space.

In this paper, volume conservation to within a tolerance of 0.02% is enforced by bounding the maximum allowable fractional change in calculated volume V_c from its initial value V_0. When this tolerance is exceeded, the initial volume is virtually restored by multiplying each nodal value of the free-surface location f (except at the fixed contact line) by a factor of $(V_0/V_c)^{1/3}$. In a series of test cases with $Re = 10$ and $A = 0.1$ using a 16×8 mesh, the resonance frequency and aspect ratios at steady state calculated with volume renormalization agreed to within four significant digits with results obtained without volume correction. It is noteworthy that with volume renormalization, the corrections made to f are limited to values that are several orders of magnitude smaller than the criteria used for convergence of the iterative technique employed for solving the discretized Navier–Stokes system and detection of limit cycles. Moreover, with the volume renormalization in place, mesh refinement tests of the type performed by W&B showed that using a 16×8 mesh produced results which agreed to within four significant digits with those obtained using finer meshes when $Re \leqslant 40$ and $A \leqslant 0.125$. The 16×8 mesh was therefore used exclusively for obtaining the computational results reported in the following sections.

3.2. *Discrete sweep algorithm*

The detection of deformation hysteresis entailed the implementation of the approach described in § 2.2. In this approach, whenever a limit cycle was detected, the entire solution $\{\boldsymbol{v}, p, f\}$ at the value of the control parameter x (Ω or A) was saved and the control parameter was increased or decreased by the specified increment Δx. If at any value of the control parameter a limit cycle was not attained before the dimensionless time measured from the attainment of the previous limit-cycle solution exceeded a prespecified maximum (here, 100), or if the algorithm failed to converge at any point, the saved solution from the last limit cycle was restored and the value of the increment in the control parameter was halved to $\Delta x/2$. The time integrations were then restarted from the value of the control parameter equal to $x \pm \Delta x/2$. If a failure occurred for a second time, the increment in the control parameter was halved one more time to $\Delta x/4$. The simulation was terminated if a failure occurred for a third time. When successful, the aforementioned discrete sweep procedure allowed a smooth transition from one steady oscillatory state to a new one with a small change in the control parameter.

4. Results and discussion

4.1. *Forced oscillation behaviour*

In the absence of flow, the equilibrium shape of a supported drop is determined by a balance between gravitational and surface tension forces. When the support is set into vertical oscillations in a time-periodic manner, viscous and inertial forces enter the picture and compete with the force of surface tension to determine the evolution in time of the drop shape and the underlying flow and pressure fields. It is instructive to view the ratio of these forces in terms of ratios of certain time scales. These are

the time scale for vorticity transport from the moving solid boundary and the time scale for rod motion, both made dimensionless by the capillary time scale, namely

$$\frac{t_v}{t_c} = \frac{R^2/v}{\sqrt{\rho R^3/\sigma}} = \frac{1}{v}\sqrt{\frac{\sigma R}{\rho}} = Re \tag{12}$$

and

$$\frac{t_r}{t_c} = \frac{1/\tilde{\Omega}}{\sqrt{\rho R^3/\sigma}} = \Omega^{-1}. \tag{13}$$

When the former ratio of time scales is held fixed, the maximum deformation $(a/b)_m$ attained by the drop during steady-state oscillations varies with the reciprocal of the latter time scale as follows. When $\Omega \ll 1$, the drop behaves as if it were a static drop and suffers little deformation regardless of the value of Re. However, as Ω is increased and the reciprocal of the dimensional time scale for rod motion becomes comparable to the natural frequency of oscillation of the drop, which is set by the capillary time scale, a forcing frequency is reached at which the deformation of the drop is maximized. The value of Ω at which this occurs is known as the primary resonance frequency $\omega_{r1} \equiv \Omega$.

Figure 3 shows the variation of maximum drop deformation $(a/b)_m$ with forcing frequency Ω for several values of Re when the forcing amplitude is held fixed at $A = 0.05$. This figure exhibits the evolution of primary resonance frequencies and the deformations suffered by the drops under resonance conditions over a small subset of the parameter space explored by W&B. As in the paper of W&B, each data point (not shown) that falls on one of the curves plotted in figure 3 has been obtained for an initially static drop that is set into motion by oscillating the supporting rod at frequency Ω. Higher-order resonance frequencies also result at higher Ω values, corresponding to the higher modes of oscillation of the supported drop (cf. Basaran 1992; W&B). Similar resonance phenomena are exhibited by liquid bridges (C&T) and levitated drops (Trinh *et al.* 1996) undergoing forced oscillations.

The insert to figure 3 shows the variation of the primary resonance frequency ω_{r1} with the Reynolds number Re. Indeed, this figure makes plain that when Re is larger than about 30, the value of ω_{r1} is insensitive to further increases in the value of Re. It is this insensitivity of ω_{r1} to changes in Re for even moderate values of the Reynolds number that renders impossible the use of simple frequency response analysis in inferring the viscosity and/or surface tension of liquids from forced oscillations of supported drops and liquid bridges (see C&T and Mollot *et al.* 1993).

Figure 3 also shows that as Re increases, namely the relative importance of forcing to damping rises, $(a/b)_m$ increases. The results of figure 3 point to the incipience of hysteresis as Re increases and the capability of simple frequency response analysis to detect an upper turning point $\omega_u \equiv \Omega_u$, if it exists, without a sweep procedure. However, to examine continuation of the upper solution branch, if it exists, to the left of ω_u and to locate the lower turning point $\omega_l \equiv \Omega_l$, the sweep procedure of the sort described in §§ 2 and 3 is needed. Moreover, it is worthwhile to investigate whether such a sweep procedure can overcome the above mentioned limitation that is inherent to the frequency response analysis in determining physical properties of supported liquid drops and bridges. In the remainder of this section, the results of such sweeps are highlighted when the relevant dimensionless groups are varied in the ranges $20 \leqslant Re \leqslant 40$, $0.05 \leqslant A \leqslant 0.125$, and $0 \leqslant G \leqslant 1$.

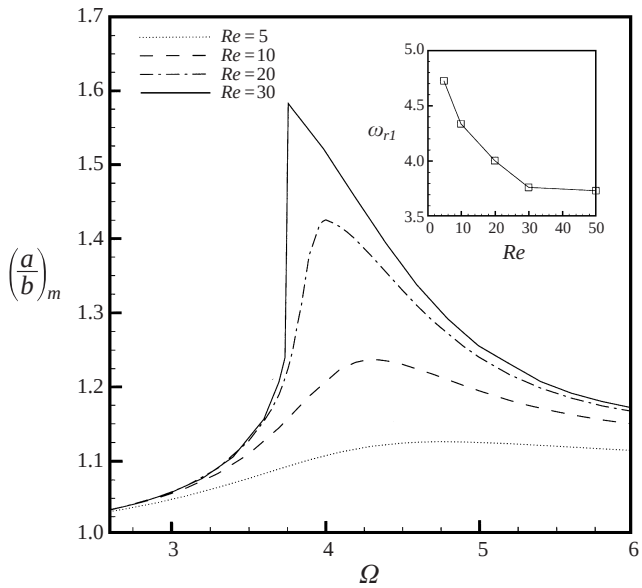

FIGURE 3. Variation of aspect ratio at maximum drop deformation $(a/b)_m$ during steady-state oscillations as a function of forcing frequency Ω in the vicinity of the primary resonance frequencies at four values of the Reynolds number Re. The deformation response profiles shown have been obtained with frequency response analysis without a sweep procedure. Here $G = 0$ and $A = 0.05$. Insert shows the variation of the primary resonance frequency ω_{r1} with Re.

4.2. *Hysteretic deformation behaviour*

Figure 4 confirms computationally that the drop response can become hysteretic when the governing dimensionless groups have values that equal those of the drop that is at the incipience of hysteresis in figure 3, i.e. for $Re = 30$ and $A = 0.05$, when the forcing frequency Ω is swept between 3.6 and 3.8 in each direction. The hysteresis range detected by the sweep procedure that is shown in figure 4 lies between $3.69 \pm 0.01 \leqslant \Omega \leqslant 3.77 \pm 0.01$. In the sweep carried out to establish the results shown in figure 4 when $3.69 \pm 0.01 \leqslant \Omega \leqslant 3.77 \pm 0.01$, the control parameter was varied in such a way that two limit cycles were found at a given value of the forcing frequency at four distinct values of Ω. As in figure 1, the lower solution branch shown in figure 4 continues up to the upper turning point $\omega_u \approx 3.77 \pm 0.01$, at which point the tangent to the curve of drop deformation versus forcing frequency becomes nearly vertical. It is noteworthy that the upper solution branch exhibits a maximum in $(a/b)_m$ at a value of the forcing frequency that lies in the hysteresis range. Indeed, $(a/b)_m$ first increases and then decreases as the forcing frequency is swept downward from its value at the upper turning point Ω_u to that at the lower turning point Ω_l. Hence whereas the maximum value of $(a/b)_m$ equals 1.573 and is attained at the resonance frequency of $\Omega = 3.80$ when classical frequency response analysis is used as in figure 3, a higher $(a/b)_m$ value of 1.586 is attained albeit at the lower value of $\Omega = 3.74$ along the upper solution branch when the sweep procedure is used. For values of Ω that lie outside the hysteresis range, the calculated values of $(a/b)_m$ as a function of Ω depicted in figure 4 agree quantitatively with those obtained without a sweep procedure (cf. figure 3). That hysteresis in drop deformation is possible at disturbance amplitudes as small as $\frac{1}{20}$th of the initial drop radius has profound implications for

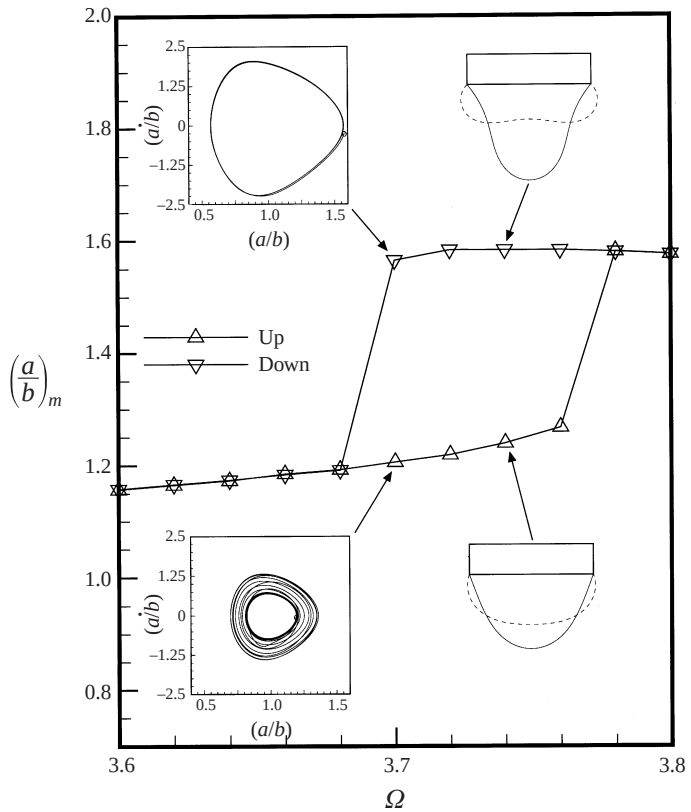

FIGURE 4. Variation of aspect ratio at maximum drop deformation $(a/b)_m$ during steady-state oscillations as a function of forcing frequency Ω. The deformation response profiles shown have been obtained with a frequency sweep. Here $Re = 30$, $G = 0$, $A = 0.05$, and Ω has been swept from 3.6 to 3.8 in both directions. The occurrence of hysteresis is indicated by the presence of two distinct solution branches for values of Ω that lie between 3.69 ± 0.01 and 3.77 ± 0.01. The shape inserts show drop profiles when the steady-state aspect ratio is maximized (solid curves) and when it is minimized (dashed curves) at $\Omega = 3.74$ along the two solution branches (see text). The phase portrait inserts show the velocity of the drop tip as a function of the position of the drop tip. Both limit cycles correspond to steady oscillatory solutions at $\Omega = 3.70$.

applications referred to in the Introduction and certain others to be discussed in the Concluding Remarks.

The shape inserts to figure 4 show drop profiles when the steady-state aspect ratio is maximized (solid curves) and minimized (dashed curves) at the same value of the forcing frequency, $\Omega = 3.74$, along both the lower branch and the upper branch of solutions. These shape inserts provide confirmation that a range of Ω exists within which the same drop may exhibit more than one stable response at the same value of the forcing frequency (and amplitude).

The attainment of each limit-cycle solution in figure 4 typically required about 500 to 1000 time steps. On an IBM RS6000-320H, which is the slowest machine that is available to us, this took about 30 to 60 minutes of CPU time. Therefore, with state-of-the-art workstations that are available today, each data point shown in figure 4 can be determined in about one tenth this time. However, because limit-cycle solutions at tens of forcing frequencies have to be determined to uncover a hysteresis

range, analysis of drop response with hysteresis can be a computationally intensive task.

Phase portraits of drop motion, such as those shown as inserts to figure 4, not only can show the existence of two distinct limit cycles at the same value of the control parameter but also can hint at the role played by initial conditions when the forcing frequency lies in the hysteresis range. In figure 4, the phase paths or trajectories shown are in the plane of the velocity of the drop tip ($\dot{a}/b$) and the normalized position of the drop tip, or aspect ratio (a/b). In figure 4, one of the phase trajectories shown is that which results when the forcing frequency is changed from 3.68 to 3.70 during an upward sweep and the other one is that obtained when the forcing frequency is changed from 3.72 to 3.70 during a downward sweep. The open circle along each of the phase trajectories corresponds to the value of tip velocity and drop aspect ratio at the point in time when the forcing frequency is either increased or decreased to 3.70 after the attainment of the previous limit cycle.

Figure 4 shows that the phase trajectory corresponding to the lower limit cycle moves away substantially from the starting point before it approaches the limit cycle at large times. Indeed, computations using different values of $\Delta\Omega$ show that the lower limit cycle can be reached from a wide range of initial conditions. By contrast, the upper limit cycle in this case occurs at a value of the forcing frequency that places it near the lower end of the upper solution branch. The upper limit cycle is attained only if the control parameter is changed by a sufficiently small amount, i.e. $\Delta\Omega \ll 1$. Computational experiments have shown that a frequency increment of 0.02 is sufficiently small in this case to allow accurate determination of the entire hysteresis range. Moreover, use of a $\Delta\Omega$ that is too large can prevent the detection of the lower turning point. Indeed use of too large a value of $\Delta\Omega$ during a downward sweep can cause either the phase trajectory to prematurely tend to the lower limit cycle or the drop to go unstable (cf. Trinh *et al.* 1996). This is a point that is returned to in what follows.

4.3. *Drop response to a frequency sweep*

According to the results shown in figure 4, the present computational method is thus capable of detecting hysteretic deformation. The effects of drop properties on this behaviour may then be examined by performing frequency sweeps at various Re values. Figure 5 shows the steady-state deformation response of drops with $Re = 20, 25, 30$, and 40 and $G = 0$ when the forcing amplitude is held fixed at $A = 0.05$ and the forcing frequency Ω is swept from 3.4 to 4.0 and then back to 3.4 as described in §§ 2 and 3. Figure 5 shows that for the most viscous drop, $Re = 20$, the drop deformation response is a single-valued function of the forcing frequency. The continuous approach to ω_{r1} from either direction further confirms that hysteresis is not achieved at this value of Re. Figure 5 shows, however, that when Re is increased to 25, two turning points appear and the drop response as measured by $(a/b)_m$ is no longer a single-valued function of Ω. The results of figure 5 indicate that when $A = 0.05$, the critical value of the Reynolds number for the onset of hysteresis is $Re = 22.5 \pm 2.5$.

Several noteworthy observations can be made upon closer examination of the results depicted in figure 5 and figures like it (see below). First, as made evident by the deformation profiles for the least viscous drops, i.e. for $Re = 30$ and 40, the values of the forcing frequency at the two turning points Ω_u and Ω_l shift toward lower values of Ω as Re increases. Second, the change in Ω_u with Re slows and approaches zero as the Reynolds number increases. Third, the value of Ω_l continues

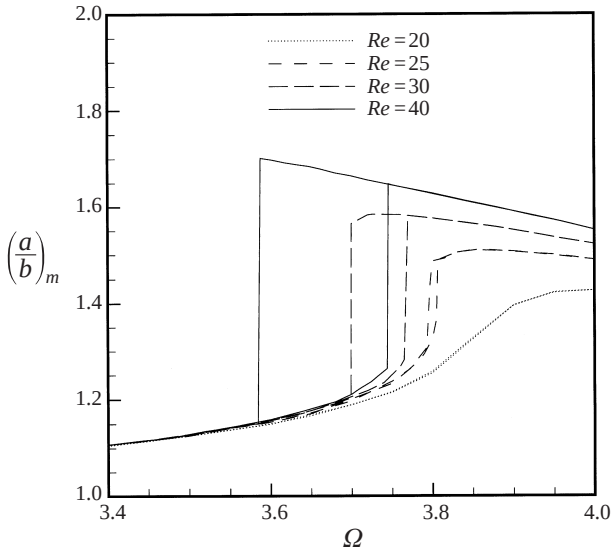

FIGURE 5. Drop response to a frequency sweep: deformation response profiles of drops for $Re = 20, 25, 30$, and 40 when $G = 0$ and $A = 0.05$.

to decrease as Re increases. Therefore, the two turning points become more widely separated from one another, or the hysteresis range $\Omega_u - \Omega_l$ widens, as Re increases. Hence, unlike ordinary frequency response analysis in which the primary resonance frequency ω_{r1} (cf. W&B and figure 3) becomes insensitive to further changes in Re when the Reynolds number is sufficiently large, the discrete sweep procedure provides a sensitive means for inferring the physical properties of the drop liquid at any value of Re. Fourth, whereas the maximum steady-state deformation $(a/b)_m$ may occur at an Ω value outside the hysteresis range when Re is moderate, it occurs inside the hysteresis range as Re gets large. Fifth, while the upward and leftward shifting of the response profiles with increasing Re is consistent with the observations of W&B (cf. figure 3), figure 5 further shows that when Re is sufficiently large the value of $(a/b)_m$ increases as Ω decreases and approaches Ω_l in the hysteresis range along the upper solution branch. This variation of $(a/b)_m$ with Ω is nearly linear, in accord with the experimental results of DePaoli *et al.* (1995) on real pendant drops but in contrast to the response exhibited by the simple Duffing oscillator (Hagedorn 1981).

Similarly, the effect of forcing amplitude on hysteretic response of oscillating pendant drops may be explored by comparing computed drop deformation profiles obtained by frequency sweeps carried out at different values of A. By way of example, figure 6 shows results of frequency sweeps obtained when $A = 0.10$ for the same values of Re as in figure 5. In both figures 5 and 6 and in all of the other cases examined (not shown), the onset of hysteresis, the location of the upper and lower turning points, and the width of a hysteresis range are also functions of A. In each case, both the hysteresis range $\Omega_u - \Omega_l$ and difference in the value of $(a/b)_m$ along the upper solution branch and that along the lower solution branch increase as either Re or A increases, in accord with intuition. Figures 5 and 6 and others like them further reveal that the limiting value of Re for onset of hysteresis decreases as A increases and that both turning points shift toward lower values of the forcing frequency as Re or A increases.

While performing frequency sweeps that resulted in figures such as 5 and 6, the

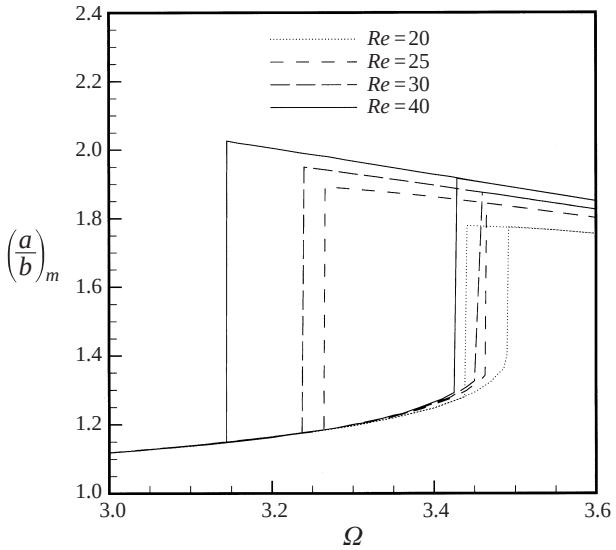

FIGURE 6. Drop response to a frequency sweep: deformation response profiles of drops for $Re = 20, 25, 30$, and 40 when $G = 0$ and $A = 0.1$.

observed value of $(a/b)_m$ sometimes jumped between the two stable solution branches for values of the forcing frequency between Ω_l and Ω_u. As alluded to earlier, the phase trajectories often tended to favour and approach the limit cycles lying on the lower solution branch. For this reason, it was often found necessary to repeat a given sweep several times using different increments in forcing frequency $\Delta\Omega$ in order to uncover in particular the extent of the upper solution branch. While the upper turning point Ω_u is also readily identified by the increasing slope of the response profile $(a/b)_m$ versus Ω as $\Omega \to \Omega_u$ from below, a similar indication of the approach to the lower turning point Ω_l was unfortunately not available due to the difficulty of detecting a decrease in the slope of the response profile as $\Omega \to \Omega_l$ from above (cf. the shapes of the response profiles in the vicinity of points B and C in figure 1). Therefore, some unavoidable uncertainty exists in the location of Ω_l values reported in this paper. However, the reported values may be considered upper bounds on the actual values.

Figure 7 shows the evolution in time of drop shapes during a single period of oscillation for a drop forced to undergo oscillations at a forcing frequency $\Omega = 3.34$ when $Re = 40$, $G = 0$, and $A = 0.10$ (cf. figure 6). Here the solid curves represent the instantaneous drop shape and the dotted curves the equilibrium drop shape which is hemispherical. Panels (*a–d*) depict drop shapes that are observed along the lower branch of solutions and panels (*e–h*) depict those that are observed along the upper branch of solutions shown in figure 6. The drop shapes depicted in panels (*a–d*), and those depicted in panels (*e–h*), are those that occur when the tip of the rod is located at $z' = -A$, 0, A, and 0, respectively, in a laboratory frame of reference. Since the number of crossings (in a quadrant) between the actual shape and the hemispherical shape furnishes the mode number of the oscillations (cf. W&B), the oscillations are purely in the primary or $n = 1$ mode for the solution lying along the lower branch. By contrast, comparison of figure 7(*g*) and the other panels along the bottom row of figure 7 reveal that there is coupling between the $n = 2$ and the $n = 1$ modes for the solution lying along the upper branch. Such mode coupling phenomena have

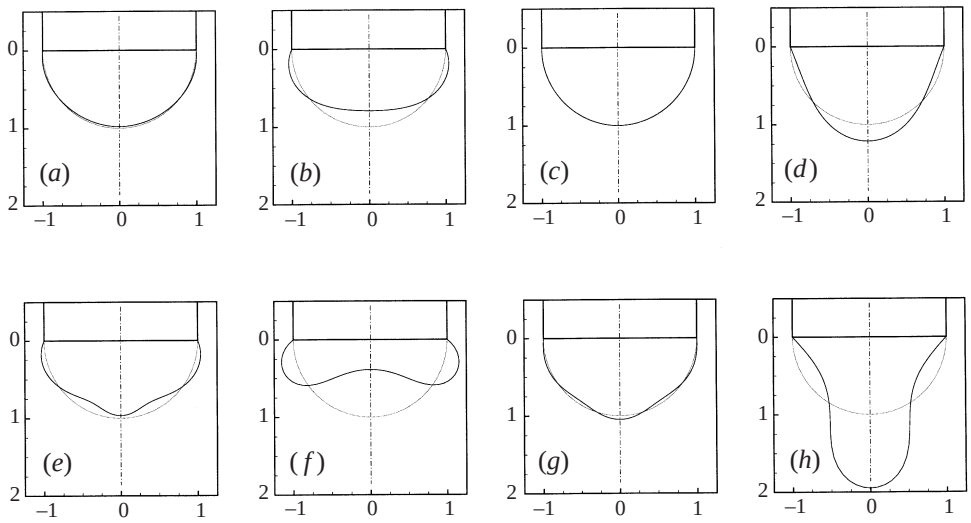

FIGURE 7. Evolution in time of drop shapes during a single period of oscillation for drops forced to undergo oscillations at a forcing frequency of $\Omega = 3.34$ when $Re = 40$, $G = 0$, and $A = 0.10$: (*a–d*) drop shapes that are observed along the lower branch of solutions and (*e–h*) drop shapes that are observed along the upper branch of solutions (see figure 6). Here the solid curves represent the instantaneous drop shape and the dotted curves the equilibrium drop shape which is hemispherical. In both rows, each drop shape shown is separated in time a quarter of a period (see text).

previously been observed in computations of large-amplitude oscillations of free drops of both inviscid (Lundgren & Mansour 1988) and viscous (Basaran 1992) liquids.

It is also instructive to contrast velocity fields within two drops at a value of the forcing frequency that lies in a hysteresis range where one of the drops falls on the lower solution branch and the other on the upper solution branch. Figures 8 and 9 show the evolution in time of the velocity fields within two drops when $\Omega = 3.74$, $Re = 30$, $A = 0.05$, and $G = 0$ (cf. figure 4). Figures 8 and 9 show the velocity field within the drop that lies along the lower and upper branches respectively of solutions in figure 4 during approximately one period after it has reached a state of steady oscillations. Although the velocity fields are plotted in the moving frame of reference, it is helpful in what follows to couch the discussion in terms of the position z' and velocity $\dot{z}'$ of the rod tip in a laboratory frame of reference. It is important to note that in figures 8 and 9, $-A \equiv -0.05 \leqslant z' \leqslant A \equiv 0.05$ and $-A\Omega \equiv -0.187 \leqslant \dot{z}' \leqslant A\Omega \equiv 0.187$.

Figure 8(*a*) shows the drop at the instant in time when the rod tip is at $z' = 0.0162$ and the rod is moving downward with velocity $\dot{z}' = 0.1769$. At this instant in time, the aspect ratio $a/b \approx 1$ and is increasing with time and the velocity vectors throughout most of the drop point in the downward direction. Figure 8(*b*) shows the drop about a quarter of a period later when the $z' \approx 0.05$ and the rod has reversed its direction of travel and is now moving upward with velocity $\dot{z}' = -0.0015$. However, because of finite inertia, fluid elements near the drop tip cannot change their direction of motion instantaneously and thus continue to move in the downward direction. In figure 8(*b*) and figure 8(*c*), where $z' = 0.0476$ and $\dot{z}' = -0.0570$, the drop deformation is near maximum. During this period when drop deformation is largest, a small recirculating eddy forms, figure 8(*b*), and grows, as shown in figure 8(*c*). The eddy has disappeared by the time the drop has reached the state depicted in figure 8(*d*), where $z' = 0.0371$

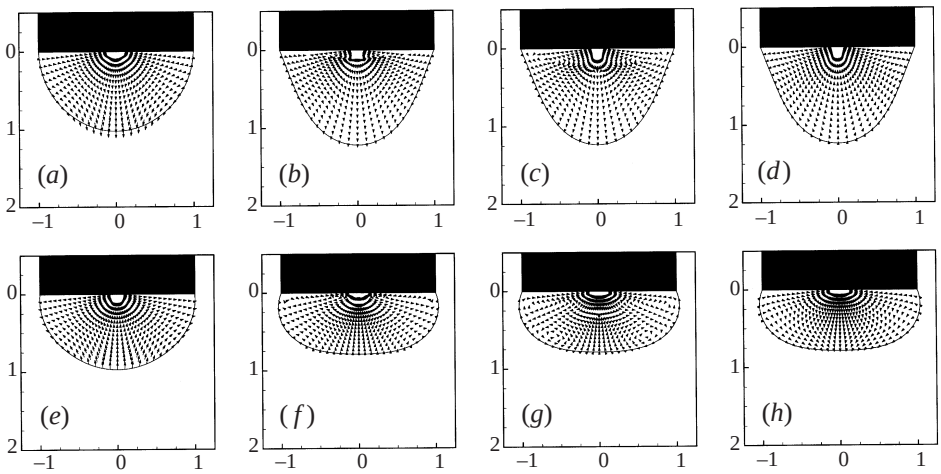

FIGURE 8. Evolution in time of the velocity field inside an oscillating supported drop with $Re = 30$, $G = 0$, $A = 0.05$, and $\Omega = 3.74$. Velocity vectors at 50% of the nodes are shown. The velocities in each of the figures have been scaled (differently) by the magnitude of the maximum velocity v_m at that time step. Each velocity vector shown belongs to its base point. (*a*) $t = 312.5675$, $a/b = 1.0218$, $v_m = 0.8460$; (*b*) $t = 312.9014$, $a/b = 1.2212$, $v_m = 0.3014$; (*c*) $t = 312.9820$, $a/b = 1.2370$, $v_m = 0.1520$; (*d*) $t = 313.0956$, $a/b = 1.2360$, $v_m = 0.1570$; (*e*) $t = 313.5416$, $a/b = 0.9744$, $v_m = 0.9163$; (*f*) $t = 313.8036$, $a/b = 0.7930$, $v_m = 0.2672$; (*g*) $t = 313.8522$, $a/b = 0.7855$, $v_m = 0.0766$; and (*h*) $t = 313.8922$, $a/b = 0.7874$, $v_m = 0.1720$. Here time is measured from the start of the sweep. Panel (*a*) represents the drop 21.4200 dimensionless time units since the frequency was changed from 3.72 to 3.74 in an upward sweep (cf. figure 4). The corresponding instantaneous positions and velocities of the rod in the laboratory frame are given in the text.

and $\dot{z}' = -0.1253$. Figure 8(*e*) shows the drop when its aspect ratio is nearly unity: at this instant $z' = -0.0370$ and $\dot{z}' = -0.1260$ and the velocity vectors throughout most of the drop point in the upward direction. By the time the drop has reached the state shown in figure 8(*f*), where $z' = -0.0486$ and $\dot{z}' = 0.0446$, the rod has already passed through the axial location where z' is a minimum and is now travelling in the downward direction again. For times corresponding to figure 8(*f–h*), the drop is near its minimum deformation. A small recirculating eddy is beginning to form near the rod surface in figure 8(*f*). In figure 8(*g*), where $z' = -0.0456$ and $\dot{z}' = 0.0766$, the eddy near the rod has grown in size and a second counter-rotating eddy has formed near the drop tip. A short time later in figure 8(*h*), where $z' = -0.0420$ and $\dot{z}' = 0.1012$, both eddies have dissipated and the velocity vectors throughout most of the drop once again point in the downward direction.

Figure 9 shows that there are some similarities and differences between the flow fields that exist within the drop that lies along the upper branch of solutions in figure 4 and those along the lower branch. As with the drop lying on the lower branch of solutions, the drop that lies on the upper branch of solutions exhibits zones of fluid recirculation when the drop is near maximum and minimum deformation, as shown in figures 9(*b–d*) and figures 9(*f*, *g*), respectively. On account of the larger deformation exhibited by the drop of figure 9 compared to the drop of figure 8, the recirculations are more intense in the former than the latter. More interestingly, figures 9(*c*) and 9(*d*) show that as the eddy near the rod when the drop is near maximum deformation dissipates, a second eddy forms near the drop tip which does not arise in the drop along the lower branch of solutions.

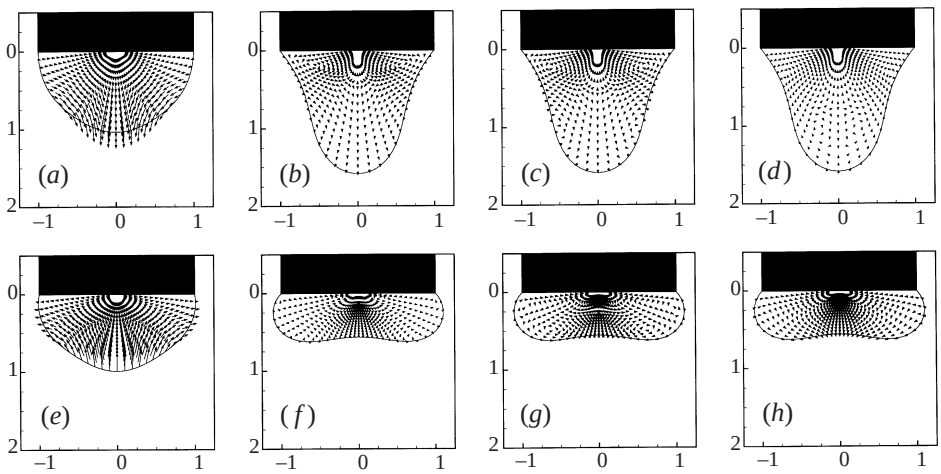

FIGURE 9. As figure 8 but for a downward sweep. (*a*) $t = 596.7386$, $z' = 0.0478$, $\overset{\circ}{z}{}' = 0.0551$, $a/b = 1.0357$, $v_m = 2.0246$; (*b*) $t = 597.2291$, $z' = 0.0018$, $\overset{\circ}{z}{}' = -0.1869$, $a/b = 1.5830$, $v_m = 0.2968$; (*c*) $t = 597.2595$, $z' = -0.0039$, $\overset{\circ}{z}{}' = -0.1864$, $a/b = 1.5861$, $v_m = 0.1909$; (*d*) $t = 597.3016$, $z' = -0.0117$, $\overset{\circ}{z}{}' = -0.1818$, $a/b = 1.5847$, $v_m = 0.1649$; (*e*) $t = 597.8113$, $z' = -0.0421$, $\overset{\circ}{z}{}' = 0.1011$, $a/b = 0.9935$, $v_m = 2.2921$; (*f*) $t = 598.0639$, $z' = -0.0028$, $\overset{\circ}{z}{}' = 0.1867$, $a/b = 0.5668$, $v_m = 0.4557$; (*g*) $t = 598.0950$, $z' = 0.0031$, $\overset{\circ}{z}{}' = 0.1867$, $a/b = 0.5582$, $v_m = 0.2321$; and (*h*) $t = 598.1273$, $z' = 0.0091$, $\overset{\circ}{z}{}' = 0.1839$, $a/b = 0.5612$, $v_m = 0.4122$. Here time is measured from the start of the sweep. Panel (*a*) represents the drop 22.6474 dimensionless time units since the frequency was changed from 3.76 to 3.74 in downward sweep (cf. figure 4).

To gain further insight into the effect of A on hysteresis phenomena during forced oscillations of pendant drops, response profiles have been obtained while holding Re and G fixed for several values of A. These calculations have shown that outside the hysteresis ranges at a given value of Ω, $(a/b)_m$ increases nearly linearly with A, in agreement with the results of W&B at low Re. In contrast to situations in which Re is varied while A is held fixed (cf. figure 5), these calculations show that both Ω_u and Ω_l depend strongly on A, while the width of the hysteresis range increases only slightly as A increases. Moreover, by carrying out sweeps at different values of A, it is straightforward to determine the critical forcing amplitude A_c above which a drop of a given Re value will undergo hysteretic deformation. Therefore, the sensitivity of the location of both turning points and the existence of a well defined value of A_c that demarcates drop response without hysteresis from that with hysteresis can both be exploited in inferring physical properties of the drop liquid.

4.4. *Drop response to an amplitude sweep*

In classical textbooks on nonlinear dynamics (see e.g. Jordan & Smith 1987), it is common to view the behaviour of a nonlinear system from a three-dimensional perspective. In the present context, this would entail determination of surfaces of constant Re in the parameter space of $\{\Omega, A, (a/b)_m\}$. So far, attention has been focused in this paper on situations in which sweeps are carried out by varying Ω while holding A fixed. To gain further insights into hysteresis phenomena associated with oscillating pendant drops and probe heretofore unexplored portions of the parameter space, results of sweeps are reported in this section in which A is varied while holding

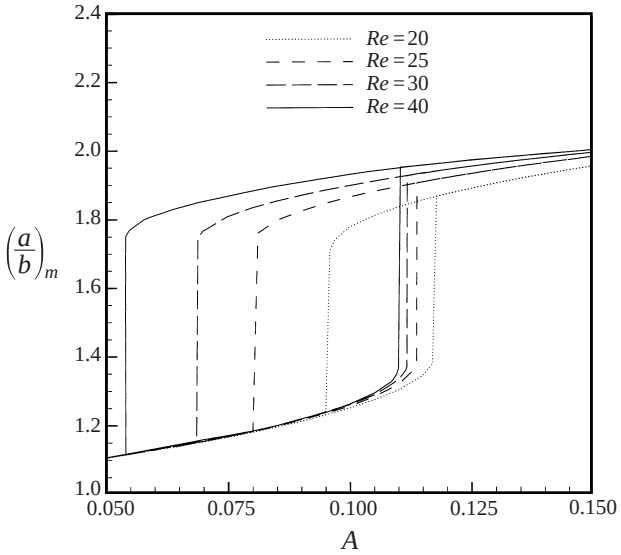

FIGURE 10. Drop response to an amplitude sweep: deformation response profiles of drops for $Re = 20, 25, 30$, and 40 when $G = 0$ and $\Omega = 3.4$.

Ω fixed. Although DePaoli *et al.* (1995) have shown through an extremely small set of experiments that hysteretic deformation can be observed experimentally during forced oscillations of a pendant drop in which the forcing amplitude is the control parameter, an adequate understanding of drop response during amplitude sweeps is lacking. Supplying this missing understanding is the goal of this section.

Figure 10 summarizes the results of amplitude sweeps performed at a fixed value of Ω of 3.4 for drops with $Re = 20, 25, 30$, and 40. In contrast to a frequency sweep in which resonance peaks can be directly observed, an amplitude sweep shows ranges of A for which the chosen Ω value lies inside or outside a hysteresis range. Inspection of figure 10 reveals that amplitude sweeps exhibit certain similarities and differences with respect to the frequency sweeps of the previous subsection. For both types of sweeps, the location of the upper turning point changes little but that of the lower turning point changes substantially as Re increases. Moreover, as Ω_u in a frequency sweep, A_u in an amplitude sweep approaches a limiting value as Re becomes sufficiently large. Nevertheless, comparison of the results of figure 10 with those of figure 6 shows that A_u is less sensitive than Ω_u to changes in Re at low Reynolds numbers. Moreover, as in frequency sweeps, the lower solution branches in amplitude sweeps nearly coincide with one another except in the vicinity of the upper turning points. Outside the hysteresis ranges, increasing Re causes a small upward shift of the upper solution branches but the magnitude of the shift falls as Re rises.

Figure 10 shows that noticeable changes in the slopes of the deformation profiles of $(a/b)_m$ versus A occur as both turning points are approached. This permits a more accurate determination of the parameter range over which hysteresis occurs in an amplitude sweep compared to a frequency sweep. Similar amplitude sweeps carried out with forcing frequency held fixed at $\Omega = 2.5$ and 5.0 (not shown) did not yield hysteretic responses, thereby confirming that all hysteresis ranges for the Re and A values examined here lie between these two extremes of forcing frequency.

Re	A_c	Ω_c
20	0.070	3.683
25	0.049	3.815
30	0.041	3.855
35	0.034	3.905
40	0.028	3.961

TABLE 1. Critical forcing amplitude and frequency at onset of hysteresis.

4.5. *Effect of gravity*

In the absence of flow, the equilibrium shape of a pendant drop of fixed volume is a function of the gravitational Bond number G and can be determined by solving the nonlinear Young–Laplace equation of capillarity (see e.g. Michael 1981). Analysis of equilibrium shapes of pendant drops of course forms the basis of a well-known technique for measuring surface or interfacial tension (e.g. Roe, Bacchetta & Wong 1967; Levin, Pitts & Terry 1976). If the rod motion is ceased during oscillations of a pendant drop, the drop shape tends to its equilibrium profile at large times. For example, the present transient algorithm predicts that the equilibrium drop aspect ratio $(a/b)_{eq}$ varies from unity at $G = 0$ to 1.0746 ± 0.0002 at $G = 1$, a result that accords with solutions of the static Young–Laplace equation.

Calculations have been carried out to determine how the drop response to a frequency sweep varies as a function of G when Re and A are held fixed. These calculations show that at low values of the forcing frequency, $(a/b)_m$ increases as gravitational Bond number G increases: this finding accords with intuition because $(a/b)_{eq}$ increases as G increases. These calculations further show that as G increases, while the width of the hysteresis range and observed $(a/b)_m$ values increase only slightly, the primary resonance frequency and the values of the upper and lower turning points decrease significantly. The downward shifting of ω_{r1}, ω_l and ω_u accords with previous studies of oscillating pendant drops (W&B) and liquid bridges (C&T) because as G increases the wavelength of a disturbance that can be accommodated between the contact line and the drop tip along the liquid–gas interface increases.

4.6. *Hysteresis ranges*

A convenient means for illustrating the ranges of forcing frequency and forcing amplitude over which hysteretic deformation may be observed during forced oscillations of a viscous supported drop of a given liquid, i.e. fixed Re, is a bifurcation diagram. In such a diagram, the values of A and Ω at which bifurcations are detected are plotted against a control parameter, here A. As part of the effort directed at constructing bifurcation diagrams, it is also desirable to determine quantitatively the critical values of forcing amplitude A_c and forcing frequency Ω_c associated with the incipience of hysteresis because the pair (A_c, Ω_c) mark the initial points of curves in such diagrams. In order to determine precise values of A_c for onset of hysteresis at several fixed values of Re, a set of frequency sweeps was performed over ranges of A in the expected vicinity of A_c. Starting at some value of the forcing amplitude A_s, frequency sweeps were performed at values of $A = A_s + 0.01\,m$, where $m = 0, 1, 2, \ldots$, until a vertical tangent was just detected in the resulting response profile. Table 1 summarizes the variation with Re of the computed values of A_c and the corresponding values of Ω_c at which the vertical tangencies were just detected. Table 1 shows that A_c falls but Ω_c rises as Re rises.

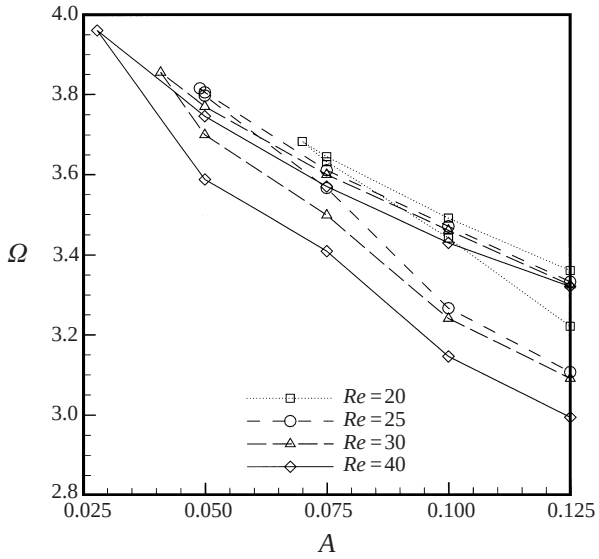

FIGURE 11. Bifurcation sets for $Re = 20, 25, 30$, and 40 when $G = 0$ showing values of (A_c, Ω_c) for onset of hysteretic drop response and evolution with forcing amplitude of locations of the two turning points between which hysteresis occurs.

Figure 11 shows the data from table 1 combined with the turning points detected over the parameter range studied in the form of bifurcation sets at four values of *Re*. In figure 11, at a fixed value of *Re*, each hysteresis range begins at (A_c, Ω_c) and hysteresis ranges corresponding to higher values of A would be represented by vertical line segments joining the upper and lower curves for the A value of interest. The bifurcation diagram reported in figure 11 conveniently shows the emergence of the turning points along with the downward shifting and widening of the hysteresis ranges with respect to forcing frequency as forcing amplitude A increases. At a given value of *Re*, the lower (upper) curve shows the lowest (highest) value of the forcing frequency at which a limit cycle could be detected along the upper (lower) solution branch. While the precision with which the lower turning points could be located is limited as previously noted, the evolution of the turning points with increasing forcing amplitude is clear. Figure 11 shows that as the drop viscosity (*Re*) decreases (increases), the forcing amplitude necessary to observe hysteretic deformation decreases. Moreover, figure 11 also makes clear that for a given value of A, the wider is the hysteresis range and the lower are the turning point frequencies the higher the Reynolds number. Although no instance of drop detachment could be detected over the range of *Re* and A examined, increasing A and/or *Re* beyond the ranges considered herein could result in the instability of oscillating pendant drops (see § 5).

According to results presented in the previous subsections, the maximum steady-state aspect ratio undergoes a large step change $\Delta(a/b)_m$ at both turning points. Figure 12(a) shows the variation of the magnitude of the step decrease in $(a/b)_m$ at the lower turning point ω_l with forcing amplitude at several values of *Re*. Figure 12(b) similarly shows the corresponding step increase at the upper turning point ω_u. In each case, the magnitudes of the step changes in drop deformation are strong functions of *Re* and increase most rapidly with A when the forcing frequency is near A_c. The soft nonlinearity of oscillating pendant drops gives rise to downward jumps in $(a/b)_m$ that are greater in magnitude than the upward jumps in $(a/b)_m$ because the amplitude of

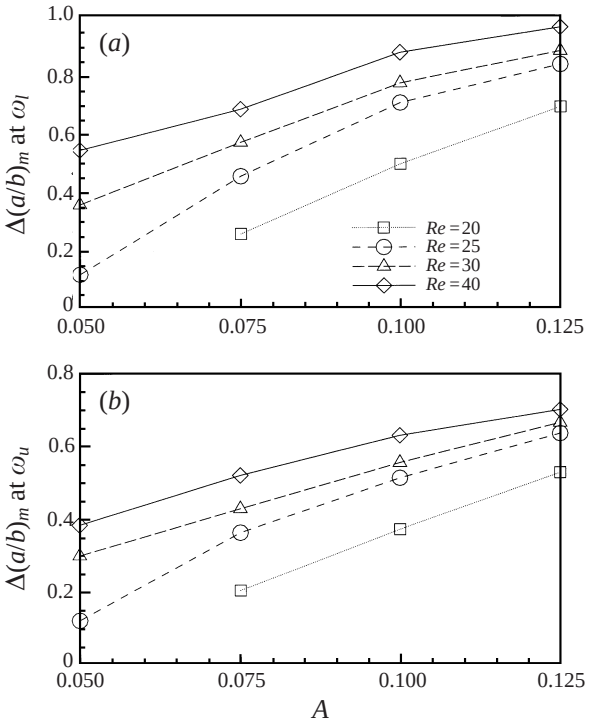

FIGURE 12. Variation with forcing amplitude of the magnitude of the step changes in $(a/b)_m$ at the two turning points for $Re = 20, 25, 30$, and 40 when $G = 0$. (*a*) $\Delta(a/b)_m$ at the lower turning point and (*b*) $\Delta(a/b)_m$ at the upper turning point.

the drop response in general increases as Ω is increased (decreased) along the lower (upper) solution branch in the hysteresis range. Understanding the variation of these step changes in response amplitude with the governing dimensionless groups is likely to prove important in practical applications.

4.7. *Forced oscillations of drops hanging from tubes*

Although supporting a drop of liquid at the tip of a rod is in principle a straightforward task (DePaoli 1994), certain factors complicate its operation in practice. First, the drop liquid must be placed on the rod by either using a syringe to deposit the drop liquid directly on it or dipping the rod into a container of the drop liquid. Either method of drop placement can result in imperfect wetting of the rod surface by the drop liquid and the violation of the fixed contact line boundary condition (cf. DePaoli 1994). Even if the contact line is pinned, it might prove difficult to deposit a drop of predetermined volume on the rod. A much easier way of creating a pendant or a sessile drop is of course to form it at the tip of a tube, as is done in the aforementioned and well-known technique for measuring surface or interfacial tension (e.g. Roe *et al.* 1967; Levin *et al.* 1976). A natural question which then arises is whether the results of frequency response analysis and frequency or amplitude sweeps would differ greatly between the situation considered earlier in this section and that of drops hanging from tubes.

The forced oscillations of supported drops hanging from tubes was analysed by modifying the algorithm for determining the response of drops hanging from rods by replacing the rod by a tube of infinitesimal wall thickness. The computational domain

in the tube problem did not terminate at $z = 0$ but extended up to a horizontal plane placed a distance $|z_i|$ upstream of the tube exit. Over the range of dimensionless groups considered, the computational results obtained with $z_i = -2$ differed by less than 0.1% from those obtained with $z_i = -8$. However, the results were sensitive to the location of the horizontal plane if $|z_i| < 2$.

By way of example, a frequency response analysis has been carried out to determine the variation of maximum drop deformation $(a/b)_m$ with forcing frequency Ω for drops that are hanging from tubes and rods for two values of Re, $Re = 10$ and 20, when the forcing amplitude is held fixed at $A = 0.05$. At both Reynolds numbers, both the deformation at resonance and the primary resonance frequency are higher for a drop hanging from a tube than one hanging from a rod. That the deformations at resonance are higher in the former case compared to those in the latter case accords with intuition because of the restraining influence of the rod surface at $z = 0$ on the motion of the fluid interface and the underlying fluid in the latter case. Moreover, that the resonance frequencies are lower in the latter case than those in the former case also accords with intuition because the presence of a no-slip boundary at $z = 0$ slows down the motion and hence increases (decreases) the period (frequency) of oscillation compared to the situation when the no-slip boundary is replaced by a liquid which is identical to that of the drop. The calculations also show that the resonace frequencies are only slightly affected if the rod is replaced by a tube. However, if the rod or the tube is impulsively brought to rest and the oscillations are allowed to decay freely (cf. Basaran & DePaoli 1994), one finds that the ensuing free oscillations are more highly damped in the presence of a rod than in the presence of a tube.

A further comparison between the two situations has been obtained by computing the steady-state deformation response of a drop hanging from a tube with $Re = 30$ and $G = 0$ when the forcing amplitude is held fixed at $A = 0.05$ and the forcing frequency Ω is swept from 3.5 to 4.0 and then back to 3.5 as described in §§ 2 and 3. The calculations have shown that drop response is hysteretic over a range of frequencies. Comparison of these results to those of figure 4 in which the dimensionless groups are identical reveals that the hysteresis range is pushed to higher values of the forcing frequency and the drop deformations in the hysteresis range are larger for a drop hanging from a tube than one hanging from a rod. Although computational results cited in this subsection and others like them show that the differences in the results of frequency response and sweep analyses between the two situations are small, care must be exercised when comparing experimental measurements and computational predictions of forced oscillations of supported drops obtained under different conditions.

5. Concluding remarks

The results of this research represent the prediction for the first time of hysteresis phenomena during forced oscillations of liquid drops and bridges by computational analysis of the full transient, nonlinear, Navier–Stokes system in more than one space dimension. The calculations reported herein have shown that hysteresis in drop deformation is possible at forcing amplitudes as small as a few percent of the undeformed drop radius, a finding which has immense implications in diverse practical applications.

Numerical analysis of the free boundary problem composed of the full, transient, nonlinear Navier–Stokes equation and associated interfacial and boundary conditions that is carried out in this paper to uncover hysteretic deformation of the free surface

shape has application in other free-surface flows. An example of a particularly important class of free-surface flows is coating flows, which are the backbone of industrial processes involved in the manufacture of X-ray and photographic film, VCR tapes, and microelectronic materials. In the study of coating flows, even if a flow is linearly stable in the theoretical sense, i.e. all small-amplitude disturbances decay in time, its sensitivity to ongoing disturbances in the operating environment is an issue of immense practical importance (see e.g. Christodoulou 1990). The sensitivity of these practically important free-surface flows to such disturbances is often evaluated by carrying out a linearized frequency response analysis. However, Giavedoni (1995) has employed the full nonlinear Navier–Stokes system as in this paper to study the stability of thin film coating flows with respect to certain high-frequency disturbances. Although this author did not find hysteresis because she did not use the sweep procedure employed in this paper, the occurrence of hysteresis can have disastrous consequences in such practical situations. For example, in a region of the parameter space over which hysteresis occurs, a coated film of a certain thickness may result during part of the process and one of drastically different thickness may be produced at other times.

There are numerous applications (see Introduction) where one would like to go beyond the stable oscillations presented in this paper and predict the onset of drop instability during forced oscillations. Although much is now known about stable oscillations of drops supported on rods (cf. W&B), studies of drop breakup during forced oscillations are only in their infancy. For example, Smith *et al.* (1998) have sidestepped the more difficult problem of modelling the breakup process and instead have resorted to correlating their experimental data on drop oscillations and breakup through the use of the simple harmonic oscillator equation. Reassuringly, the numerical methods presented in this paper can be extended (Wilkes, Phillips & Basaran 1998) to analyse without any *ad hoc* approximations the more complicated problem of drop ejection from an oscillating rod (Wilkes & Basaran 1998).

The authors thank Dr R. M. Wham of Oak Ridge National Laboratory for access to his IBM RS6000 workstation on which some of the extensive computations necessary for this study were carried out. This research was sponsored by the NASA Microgravity Science and Applications Division and the Shell Doctoral Fellowship Program (E. D. W.).

REFERENCES

Basaran, O. A. 1992 Nonlinear oscillations of viscous liquid drops. *J. Fluid Mech.* **241**, 169.

Basaran, O. A. & DePaoli, D. W. 1994 Nonlinear oscillations of pendant drops. *Phys. Fluids* **6**, 2923.

Borkar, A. & Tsamopoulos, J. 1991 Boundary-layer analysis of the dynamics of axisymmetric capillary bridges. *Phys. Fluids* A **3**, 2866.

Chang, C.-H. & Franses, E. I. 1994*a* An analysis of the factors affecting dynamic tension measurements with the pulsating bubble surfactometer. *J. Colloid Interface Sci.* **164**, 107.

Chang, C.-H. & Franses, E. I. 1994*b* Dynamic tension behavior of aqueous octanol solutions under constant-area and pulsating-area conditions. *Chem. Engng Sci.* **49**, 313.

Chen, T.-Y. & Tsamopoulos, J. 1993 Nonlinear dynamics of capillary bridges: theory. *J. Fluid Mech.* **255**, 373 (referred to herein as C&T).

Chen, T.-Y., Tsamopoulos, J. A. & Good, R. J. 1992 Capillary bridges between parallel and non-parallel surfaces and their stability. *J. Colloid Interface Sci.* **151**, 49.

Christodoulou, K. N. 1990 Computational physics of slide coating flow. PhD thesis, University of Minnesota.

Daidžić, N. 1995 Nichtlineare Tropfenschwingungen und -verdampfung in einem Ultraschall-Positionierer. PhD thesis, Universität Erlangen-Nürnberg.

DePaoli, D. W. 1994 Linear and nonlinear behavior of oscillating pendant drops. PhD thesis, University of Tennessee.

DePaoli, D. W., Feng, J. Q., Basaran, O. A. & Scott, T. C. 1995 Hysteresis in forced oscillations of pendant drops. *Phys. Fluids* **7**, 1181.

DePaoli, D. W., Scott, T. C. & Basaran, O. A. 1992 Oscillation frequencies of droplets held pendant on a nozzle. *Sep. Sci. Technol.* **27**, 2071.

Giavedoni, M. D. 1995 A numerical study of the two-dimensional thin liquid film subject to a vertical oscillation. *Indust. Engng Chem. Res.* **34**, 356.

Hagedorn, P. 1981 *Non-Linear Oscillations.* Clarendon.

Harris, M. T., Scott, T. C. & Byers, C. H. 1992 Method and apparatus for the production of metal oxide powder. US Patent 5,122,360 (June 16, 1992).

Jordan, D. W. & Smith, P. 1987 *Nonlinear Ordinary Differential Equations*, 2nd Edn. Clarendon.

Kistler, S. F. & Scriven, L. E. 1983 Coating flows. In *Computational Analysis of Polymer Processing*, (ed. J. R. A. Pearson & S. M. Richardson), p. 243. Applied Science Publishers, London.

Koizumi, T., Shibazaki, H., Nishio, T. & Nishiwaki, N. 1983 Study of rolling friction – behaviour of the small displacement of starting rolling friction. *Wear* **88**, 285.

Królikowski, W. & Cronin-Golomb, M. 1991 Optical bistability in the semilinear phase-conjugate mirror. *Appl. Phys.* B **52**, 150.

Levin, P. F., Pitts, E. & Terry, G. C. 1976 New method for measuring surface tension from the height of a pendent drop. *J. Chem. Soc. Faraday Trans.* I **72**, 1519.

Lundgren, T. S. & Mansour, N. N. 1988 Oscillations of drops in zero gravity with weak viscous effects. *J. Fluid Mech.* **194**, 479.

Michael, D. H. 1981 Meniscus stability. *Ann. Rev. Fluid Mech.* **13**, 189.

Mollot, D. J., Tsamopoulos, J., Chen, T.-Y. & Ashgriz, A. 1993 Nonlinear dynamics of capillary bridges: experiments. *J. Fluid Mech.* **255**, 411.

Parlitz, U., Englisch, V., Scheffczyk, C. & Lauterborn, W. 1990 Bifurcation structures of bubble oscillators. *J. Acoust. Soc. Am.* **88**, 1061.

Pezeshki, C., Elgar, S. & Krishna, R. C. 1991 An examination of multi-frequency excitation of the buckled beam. *J. Sound Vib.* **148**, 1.

Ptasinski, K. J. & Kerkhof, P. J. A. M. 1992 Electric field driven separations: phenomena and applications. *Sep. Sci. Technol.* **27**, 995.

Roe, R.-J., Bacchetta, V. L. & Wong, P. M. G. 1967 Refinement of pendent drop method for the measurement of surface tension of viscous liquid. *J. Phys. Chem.* **71**, 4190.

Salehpour, A. & Yao, S.-C. 1983 Thermal hysteresis of forced convective boiling. *Intl J. Multiphase Flow* **9**, 97.

Scott, T. C. & Wham, R. M. 1988 Surface area generation and droplet size control in solvent extraction systems utilizing high intensity electric fields. US Patent 4,767,515 (August 30, 1988).

Shaw, J. & Shaw, S. W. 1991 Non-linear resonance on an unbalanced rotating shaft with internal damping. *J. Sound Vib.* **147**, 435.

Smith, M. K., James, A., Vukasinovic, B. & Glezer, A. 1998 Vibration-induced droplet atomization. *Fourth Microgravity Fluid Physics and Transport Phenomena Conf., Cleveland, Ohio, 12–14 August 1998.* NASA.

Trinh, E. H., Holt, R. G. & Thiessen, D. B. 1996 The dynamics of ultrasonically levitated drops in an electric field. *Phys. Fluids* **8**, 43.

Tsamopoulos, J., Chen, T.-Y. & Borkar, A. 1992 Viscous oscillations of capillary bridges. *J. Fluid Mech.* **235**, 579.

Wilkes, E. D. & Basaran, O. A. 1997 Forced oscillations of pendant (sessile) drops. *Phys. Fluids* **9**, 1512 (referred to herein as W&B).

Wilkes, E. D. & Basaran, O. A. 1998 Drop ejection from an oscillating rod. *Fourth Microgravity Fluid Physics and Transport Phenomena Conf., Cleveland, Ohio, 12–14 August 1998.* NASA.

Wilkes, E. D., Phillips, S. D. & Basaran, O. A. 1998 Computational and experimental analysis of dynamics of drop formation. Submitted to *Phys. Fluids.*